Comparison of Functional Network Connectivity and Granger Causality for Resting State fMRI Data

Ce Zhang[1], Qiu-Hua Lin[1(✉)], Chao-Ying Zhang[1,2,3,4,5], Ying-Guang Hao[1], Xiao-Feng Gong[1], Fengyu Cong[2,3], and Vince D. Calhoun[4,5]

[1] School of Information and Communication Engineering, Dalian University of Technology, Dalian 116024, China
qhlin@dlut.edu.cn
[2] Department of Biomedical Engineering, Dalian University of Technology, Dalian, China
[3] Department of Mathematical Information Technology, University of Jyvaskyla, Jyväskylä, Finland
[4] The Mind Research Network, Albuquerque, NM 87106, USA
[5] Department of Electrical and Computer Engineering, University of New Mexico, Albuquerque, NM 87131, USA

Abstract. Functional network connectivity (FNC) and Granger causality have been widely used to identify functional and effective connectivity for resting functional magnetic resonance imaging (fMRI) data. However, the relationship between these two approaches is still unclear, making it difficult to compare results. In this study, we investigate the relationship by constraining the FNC lags and the causality coherences for analyzing resting state fMRI data. The two techniques were applied respectively to examine the connectivity within default mode network related components extracted by group independent component analysis. The results show that FNC and Granger causality provide complementary results. In addition, when the temporal delays between two nodes were larger and the causality coherences were distinct, the two approaches exhibit consistent functional and effective connectivity. The consensus between the two approaches provides additional confidence in the results and provides a link between functional and effective connectivity.

Keywords: Functional network connectivity · Granger causality · Resting state fMRI · Group ICA · Default mode network

1 Introduction

Over the past decades, an increasing number of analytical methods have been introduced to explore the functional and effective connectivity among brain functional networks [1, 2]. Functional network connectivity (FNC) is a powerful functional connectivity approach for assessing temporal coherence among brain networks by utilizing lag shift correlations between nodes [3]. On the other side, as a typical method for effective

F. Cong et al. (Eds.): ISNN 2017, Part II, LNCS 10262, pp. 559–566, 2017.
DOI: 10.1007/978-3-319-59081-3_65

connectivity, Granger causality is a statistical method for exploring the predictability and dependencies to establish causal relationships between brain networks [4].

FNC and Granger causality have been separately applied to fMRI data for identifying typical resting connectivity networks. In particular, FNC had been used to distinguish the abnormal relationships among several specific networks in psychiatric patients from the normal controls [5, 6]. Comparisons of functional network connectivity during resting and task conditions showed that functional network connectivity was stronger during rest compared to task [7]. As for Granger causality, its investigation for functional brain organization also found that schizophrenia patients exhibited significantly enhanced causal influence between specific regions [4, 8, 9].

Quite recently, FNC and Granger causality have both been utilized for analyzing connectivity changes among different age stages based on resting and task fMRI data [10]. FNC was employed to detect internetwork connectivity between the salience network, executive control networks and default mode networks (DMNs), while Granger causality was used to analyze the effective connectivity. In [10], FNC and Granger causality were used as two entirely different approaches with no analysis about connections between their results. As such, this study aims to directly compare the two approaches and examine how to leverage any complementary information they provide about the data. Eighty-two subjects of resting state fMRI data were used in the comparative analyses.

The rest of this paper is organized as follows. Section 2 introduces the resting state fMRI data we used, the components we extracted, and the two key algorithms: FNC and Granger causality. In Sect. 3, we presented the results of the two approaches, and compared the results of FNC under different time-lags and those of Granger causality with causality coherence constraint. Section 4 has the conclusions.

2 Methods

2.1 Materials

The fMRI Data from 82 subjects were collected using a 3T Siemens Trio scanner with the parameters: repeat time (TR) = 2 s, echo time = 29 ms, field of view = 240 mm, flip angle = 75º, slice thickness = 3.5 mm, gap = 1.05 mm, matrix size = 64 × 64 33, voxel size = 3.75 × 3.75 × 4.55 mm^3, number of timepoints = 150. All subjects were instructed to do nothing but keep their eyes open during the scan. Data were preprocessed using the statistical parametric mapping (SPM) software package. After motion correction, spatial normalization with isotropic resampling to voxels of 4 × 4×4 mm^3 in standard Montreal Neurological Institute brain space, and spatial smoothing with an 8 mm full width at half maximum Gaussian kernel, we obtained fMRI datasets with dimension 53 × 53 × 46 × 150 for each subject.

2.2 Extraction of Components

Spatial group independent component analysis (ICA), which has been widely used for extracting components from fMRI data, was performed for all 82 subjects using the

toolbox GIFT (http://mialab.mrn.org/software/gift) [11]. Since high model order enables us to evaluate multiple sub-networks within each network domain [12], we separated 120 independent components (IC) using the Infomax algorithm. After ICA separation, we further extracted seven DMN-related components based on their spatial map references [13]. These components, as shown in Fig. 1, were medial prefrontal cortex (MPFC) corresponding to IC10, left and right inferior parietal lobule (IPL) corresponding to IC80, IC16, and posterior cingulate cortex (PCC) corresponding to IC22, IC52, IC66, and IC71. Prior to being applied to FNC and Granger causality, the time courses of these seven DMN-related components were low-pass filtered (Butterworth, cutoff frequency 0.15 Hz).

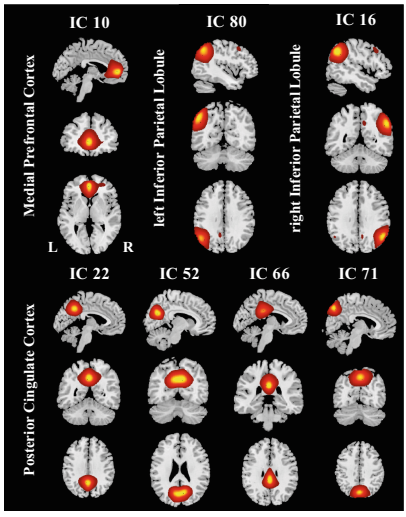

Fig. 1. Spatial maps of the seven DMN-related components. The final spatial maps were z-scored and thresholded at $|Z| \geq 2$ and displayed at the three most informative slices.

2.3 Functional Network Connectivity (FNC)

FNC computes the lag-shift Pearson's correlation coefficient between pairs of time courses using the FNC toolbox (http://mialab.mrn.org/software):

$$\rho_{\Delta t} = \frac{X_{t_0}^T Y_{t_0+\Delta t}}{\sqrt{X_{t_0}^T X_{t_0}} \times \sqrt{Y_{t_0+\Delta t}^T Y_{t_0+\Delta t}}} \tag{1}$$

where $\rho_{\Delta t}$ represents correlation between two time courses X and Y, while Δt stands for the time shifting from the initial reference point t_0. FNC recorded the maximal lagged correlation $\rho_{\max}^{(k)} = \max\{\rho_{\Delta t}\}$ and its corresponding lag $\Delta t^{(k)}$ for a single subject k, $k = 1, \ldots, K$ (K is the number of subjects), and then averaged across all subjects. The statistical significance of these correlations and lags was finally calculated by using one sample t-test at $p < 0.05$ corrected by false discovery rate (FDR), respectively [3].

2.4 Granger Causality

Granger causality relies on linear regression models of a stochastic process. Specifically, if the information in the past of a time series can be used to improve the prediction accuracy of the future of another time series, then the former is the Granger cause of the latter. Let X_t, Y_t be two stationary variables, i.e., the two time courses here, the autoregressive model can be described as:

$$X_t = \sum_{j=1}^{m} a_j X_{t-j} + \sum_{j=1}^{m} b_j Y_{t-j} + \varepsilon_t, \quad Y_t = \sum_{j=1}^{m} c_j X_{t-j} + \sum_{j=1}^{m} d_j Y_{t-j} + \eta_t \tag{2}$$

where a_j, b_j, c_j, and d_j are best fit regressors of the model, ε_t and η_t are two zero-mean uncorrelated white-noise series. The model order m can be determined by MDL criterion. The measure of the strength of the causality $X \rightarrow Y$ can be defined as,

$$C_{\overrightarrow{xy}} = \frac{\sigma_\varepsilon^4 |(1-d)c|^2}{(\sigma_\varepsilon^2 |(1-d)|^2 + \sigma_\eta^2 |(b)|^2)(\sigma_\varepsilon^2 |(c)|^2 + \sigma_\eta^2 |(1-a)|^2)} \tag{3}$$

Similarly, the measure of the strength of the causality $Y \rightarrow X$ ($C_{\overrightarrow{yx}}$) can be defined with another numerator $\sigma_\eta^4 |(1-a)b|^2$. We call ($C_{\overrightarrow{xy}}$) and ($C_{\overrightarrow{yx}}$) the causality coherences. It should be noted that $0 < (C_{\overrightarrow{xy}}) < 1$ and similarly for ($C_{\overrightarrow{yx}}$) [4, 14]. The causality coherences were computed for all subjects and then averaged. After performing one sample t-test ($p < 0.05$, corrected by FDR), the directional influence between two components adopted the statistically significant causality with larger values.

3 Results

3.1 FNC and Granger Without Lag and Causality Coherence Constraints

Figure 2 demonstrates the results for FNC and Granger causality. The direction of an arrow in FNC results indicates the time delay between two components. For example, in Fig. 2(a), an arrow from IC10 to IC71 represents that IC10 precedes IC71 by certain time units. Meanwhile, in Granger causality, Fig. 2(b), an arrow IC10 → IC71 represents IC10 is the Granger cause of IC71.

For the FNC results shown in Fig. 2(a), the temporal correlations existed in every pair of components and the time-lags varied in a large range from 0.0015 s to 0.650 s. Causality was found in a subset of the components, as shown in Fig. 2(b). IC80 and IC16 (bilateral IPL) were the Granger cause of IC66 and IC71 (PCC), and IC10 (MPFC) caused IC71 (PCC), which suggests that in the DMN, the PCC may work as a special node that seldom generate but mostly receives Granger connections. The internal connection of PCC shows that IC22 caused IC71, and IC52 was the Granger cause of IC66 and IC71.

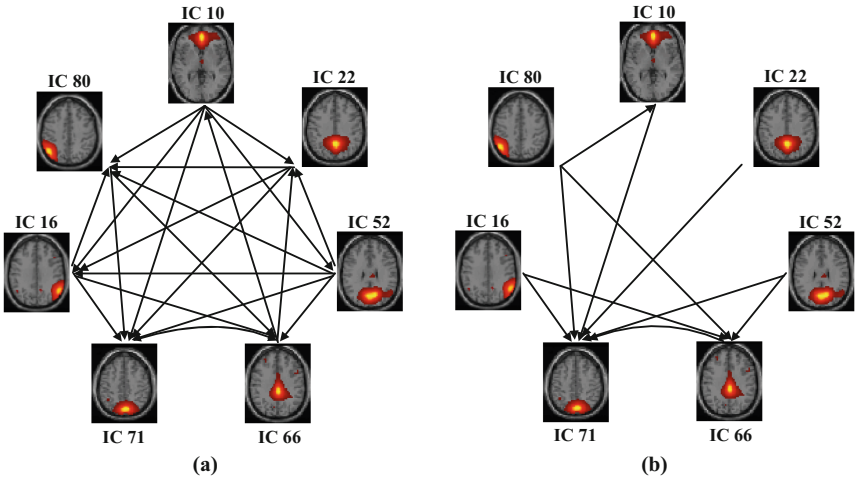

Fig. 2. Results for FNC and Granger. (a) Functional connectivity detected by FNC. (b) Effective connectivity detected by Granger causality.

When we focused on the common connectivity in both, it was not difficult to find most connections showed the same directionality. For example, IC71 and IC66 which lagged to IC80 and IC16 (bilateral IPL) in functional network connectivity were also identified as caused by them in the Granger causality approach. This was also true of connections within the PCC.

Nevertheless, it is obvious that the number of significant connections identified by FNC was much larger than that in Granger causality, and there were also a few discrepancies. The arrow direction was reverse for connections IC80 - IC10 as well as IC66 - IC71. As such, we next added constraints to the lags and causality coherences to investigate their influence on the connectivity.

3.2 FNC with Lag Constraints

In the analysis of FNC, correlation and lag values were simultaneously examined for possible combinations, and the lag markers reflected the chronological order of the related components. Considering that a small latency in FNC may be influenced by noise in the time courses and thus hard to show precedence relationship in time, we ignored lags less than 0.05 s in functional network connectivity. Figure 3 shows the results. In Fig. 3(a), the values on the line represent the 'lag (second)/correlation coefficient' between two connected components. Moreover, in Fig. 3(b) the arrow A → B is also expressed by the values of '$C_{\overrightarrow{AB}}/C_{\overrightarrow{BA}}$'.

After omitting the connections with small lags, we found that there were only ten connections left in functional network connectivity and each of them corresponded to a specific connectivity in Granger causality. The directional connectivity between components obtained from FNC was quite similar to the directionality obtained from

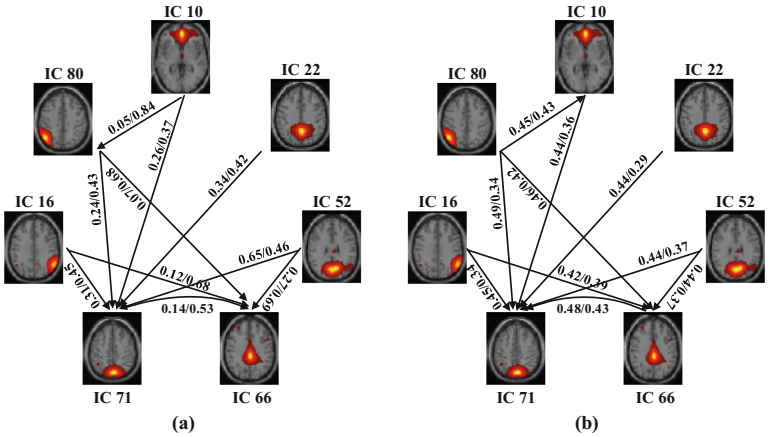

Fig. 3. Comparison of FNC and Granger with lag constraints. (a) Functional connectivity detected by FNC ignoring lags less than 0.05 s. (b) Effective connectivity detected by Granger causality. Values on the line represent 'lag (second)/correlation coefficient' in (a), while on the arrow A → B also express '$C_{\overrightarrow{AB}}/C_{\overrightarrow{BA}}$' in (b).

Granger causality: there were 8/10 connections exhibiting a close correspondence between time delay and causality. Two of the ten connections, those between IC80 - IC10 and IC66 - IC71, showed reverse directions.

It was easy to see that the time delays between IC80 - IC10 and IC66 - IC71 were also small (0.05 s for IC80 - IC10 and 0.14 s for IC66 - IC71). In addition, the difference between the causality coherences '$C_{\overrightarrow{AB}}/C_{\overrightarrow{BA}}$' was also small (less than or equal to 0.05). We further constrained lags or causality coherences in order to focus on consistent connectivity.

3.3 FNC and Granger with Both Lag and Causality Coherence Constraints

Figure 4 illustrates the results of FNC and Granger causality with both lag and causality coherence constraints. We ignored FNC connections with lags less than 0.15 s and kept Granger causality connections with '$C_{\overrightarrow{AB}}/C_{\overrightarrow{BA}}$' difference greater than 0.05. Taking the causality from A to B as an example, we find the causality is distinct when $C_{\overrightarrow{AB}} - C_{\overrightarrow{BA}} > 0.05$.

After selecting the connections with large lags and distinct causality, we found that the directional functional connectivity obtained from FNC had the same directionality obtained from Granger causality. As shown in Fig. 4, the bilateral IPL (IC16, IC80) and the MPFC (IC10) actually preceded and caused IC71 of PCC. The direction within the PCC showed consistent results in both FNC and Granger causality, which implied in the DMN some specific components of PCC were in charge of receiving connections from others. Ultimately, six connections with effective lags or causality were left, in

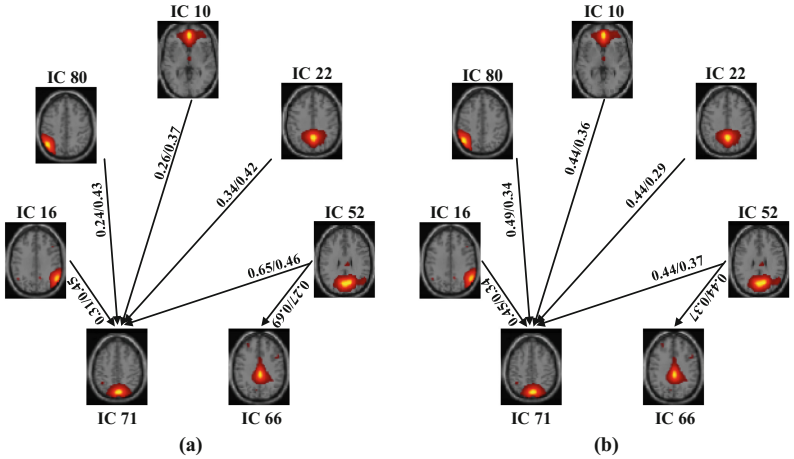

Fig. 4. Comparison of FNC and Granger with lag constraints. (a) Functional connectivity ignoring lags less than 0.15 s. (b) Effective connectivity with '$C_{\overrightarrow{AB}}/C_{\overrightarrow{BA}}$' difference greater than 0.05. Values on the line represent 'lag (second)/correlation coefficient' in (a), while on the arrow A → B also express '$C_{\overrightarrow{AB}}/C_{\overrightarrow{BA}}$' in (b).

which the two approaches can give consistent results. These results show that for these cases the lags and causality coherences are more reliable for assessing temporal and causal relationship between components than small ones which may be influenced by noise. The consistent connections identified by both methods provide reliable and stable results for estimating functional and effective connectivity.

4 Conclusions

The FNC approach detects the maximal shift lagged correlations between all pair-wise components, while the Granger causality analyzes the causal relationship between components. Previously, the two approaches have been used to detect distinct functional connectivity and effective connectivity. In this study we compared the two approaches by constraining the FNC lags and the causality coherences. When we removed small FNC lags and causality coherences, we obtained consistent functional and effective connectivity based on resting state fMRI data. The results support the conclusion that time delay has a specific meaning to the Granger causality and is a main factor driving the results. Our results also suggest that additional advantages can be gained by using FNC and Granger causality in combination. We obtain unique information from each approach, i.e., the correlation structure detected by FNC when the lags are small, and the causal relationship found by Granger causality when the difference between two reversing causality coherences is small, but also the convergent information identified by both methods provides reliable and stable information for enhancing the analysis of functional and effective connectivity. In the future, we will test how the two approaches are connected in task fMRI data.

Acknowledgments. This work was supported by National Natural Science Foundation of China under Grants 61379012, 61671106, and 81471742, NSF grants 0840895 and 0715022, NIH grants R01EB005846 and 5P20GM103472, the Fundamental Research Funds for the Central Universities (China, DUT14RC(3)037), and the China Scholarship Council.

References

1. Friston, K.J.: Functional and effective connectivity in neuroimaging: a synthesis. Hum. Brain Mapp. **2**(1–2), 56–78 (1994)
2. Greicius, M.D., Srivastava, G., Reiss, A.L., Menon, V., Raichle, M.E.: Default-mode network activity distinguishes Alzheimer's disease from healthy aging: evidence from functional MRI. Proc. Natl. Acad. Sci. U.S.A. **101**(13), 4637–4642 (2004)
3. Jafri, M.J., Pearlson, G.D., Stevens, M., Calhoun, V.D.: A method for functional network connectivity among spatially independent resting-state components in schizophrenia. NeuroImage **39**(4), 1666–1681 (2008)
4. Demirci, O., Stevens, M.C., Andreasen, N.C., Michael, A., Liu, J., While, T., Pearlson, G. D., Clark, V.P., Calhoun, V.D.: Investigation of relationships between fMRI brain networks in the spectral domain using ICA and Granger causality reveals distinct differences between schizophrenia patients and healthy controls. NeuroImage **46**(2), 419–431 (2009)
5. Allen, E.A., Erhardt, E.B., Damaraju, E., Gruner, W., Segall, J.M., Silva, R.F., et al.: A baseline for the multivariate comparison of resting-state networks. Front. Syst. Neurosci. **5**, 2 (2011)
6. Das, P., Calhoun, V.D., Malhi, G.S.: Bipolar and borderline patients display differential patterns of functional connectivity among resting state networks. NeuroImage **98**, 73–81 (2014)
7. Arbabshirani, M.R., Havlicek, M., Kiehl, K.A., Pearlson, G.D., Calhoun, V.D.: Functional network connectivity during rest and task conditions: a comparative study. Hum. Brain Mapp. **34**(11), 2959–2971 (2013)
8. Palaniyappan, L., Simmonite, M., White, T.P., Liddle, E.B., Liddle, P.F.: Neural primacy of the salience processing system in schizophrenia. Neuron **79**(4), 814–828 (2013)
9. Potvin, S., Lungu, O., Tikàsz, A., Mendrek, A.: Abnormal effective fronto-limbic connectivity during emotion processing in schizophrenia. Prog. Neuropsychopharmacol. Biol. Psychiatry **72**, 1–8 (2017)
10. Archer, J.A., Lee, A., Qiu, A., Chen, S.H.A.: A comprehensive analysis of connectivity and aging over the adult life span. Brain Connect. **6**(2), 169–185 (2016)
11. Calhoun, V.D., Adali, T., Pearlson, G.D., Pekar, J.J.: A method for making group inferences from functional MRI data using independent component analysis. Hum. Brain Mapp. **14**(3), 140–151 (2001)
12. Abou-Elseoud, A., Starck, T., Remes, J., Nikkinen, J., Tervonen, O., Kiviniemi, V.: The effect of model order selection in group PICA. Hum. Brain Mapp. **31**(8), 1207–1216 (2010)
13. Smith, S.M., Fox, P.T., Miller, K.L., Glahn, D.C., Fox, P.M., Mackay, C.E., et al.: Correspondence of the brain's functional architecture during activation and rest. Proc. Natl. Acad. Sci. U.S.A. **106**(31), 13040–13045 (2009)
14. Granger, C.W.J.: Investigating causal relations by econometric models and cross-spectral methods. Econometrica **37**(3), 424–438 (1969)